Effect of partial replacement of selenium by lead on electrical properties of $S_{70}Se_{30-x}Pb_x$ of chalcogenide glasses

Mahmoud Yousif Hajem[1, a)] and Kareem Ali Jasim[1, b)], Chafic Salame [2, c)]

[1] *Department of Physics, College of Education for Pure Science (Ibn Al-Haitham), University of Baghdad. Baghdad, Iraq*
[2]*European Academy for Sustainable Development, EURACA, 11 Rempart Saint Theibault, 57000 Metz, France*

[a)] *Mahmoud.yousif2304@ihcoedu.uobaghdad.edu.iq*
[b)] *Corresponding author: kareem.a.j@ihcoedu.uobaghdad.edu.iq*
[c)] *chafic.salame@euraca.edu.eu*

Abstract. This study involved preparing five samples of the alloy $S_{70}Se_{30-x}Pb_x$ with varying lead concentrations (x = 0, 5, 10, 15) using the melting point method, which involved partial replacement of selenium with lead. The electrical properties of the five samples were studied according to the replacement percentage. The electrical conductivity analysis revealed changes in the electrical properties of all samples due to the rearrangement of the amorphous material structure, and three different conduction mechanisms were identified. At low temperatures, electron mobility was achieved by hopping between local states close to the Fermi energy. At medium temperatures, conduction occurred by transferring electrons between local levels within the conduction and valence bands. At high temperatures, electrons were transferred through extended levels within these two bands. The results showed that the calculated densities of states for localized, extended, and near-Fermi states change with the lead concentration.

Keywords: Alloy, lead concentrations, Electrical conductivity, electron mobility, hopping electron, localized and extended.

INTRODUCTION

Amorphous chalcogenide semiconductors have been widely studied and often exhibit typical P-type behavior characteristics, largely due to the abundance of localized states near the Fermi energy and within the energy gap, where the Fermi level is effectively stabilized by the abundance of localized states [1-3]. These materials become more amenable to technological applications when metal additives or partial replacement of their chemical components are added [4], which enhances their conductivity and significantly reduces the activation energy required for conduction [5]. According to the Mott-Davies model, the valence requirements of Chalcogenides are usually met for all elements [6]. This model explains the subtle changes in electrical and optical behavior in doped and undoped chalcogenides. Studies have shown that the introduction of some chemical elements, such as Bismuth, can significantly enhance the conductivity of P-type, increasing it by more than 7% compared to N-type materials [7]. On the other hand, the addition of elements such as indium, antimony, or tin generally results in the formation of P-type compounds [8, 9]. Since all impurities are electrically active, the concentration of impurities is a crucial factor in determining their effect [10, 11]. Therefore, understanding the effect of impurities on the properties of chalcogen glasses is essential for both theoretical and applied research [12, 13]. Experimental evidence indicates that the introduction of impurities into binary systems such as Se-Te-Sn or Ge-Te-Sb significantly alters the electrical properties of chalcogen glasses [14]. In addition, the glass composition, impurity chemistry, and doping methods have a significant impact on the behavior of the material [15]. For example, Aqeel N. Abdul Latif et al. studied the effect of indium on the density of local, extended, and Fermi-level states, revealing a change in the density of extended, local, and Fermi-level states upon increasing indium concentrations for the Se85Te10Sn5-xInx alloy to include changes in activation energy, tail width, and interstate distance, as well as an increase in the density of extended, local, and Fermi-level states [14]. When the Ge30Te70-xSbx alloy was partially replaced, the density of local and extended states and at the Fermi level were examined and it was found that all energy states including activation energy, tail width, interatomic distances and transition distance were changed [15]. Researchers [10-13] focused on studying the electrical properties of $Se_6Te_{4-x}Sb_x$ and $Se_6Te_{4-x}Snx$ alloys by partially replacing tellurium with antimony, and the energy density of several energy states was calculated, including the electronic hopping distance, Fermi level, locality, and tail width. They concluded that the density of energy states increases with the change in the concentration of the substituted elements. One of the distinctive properties of amorphous chalcogen semiconductors is their sensitivity to

external influences, especially ionizing radiation with medium energy exceeding 1 MeV [16, 17]. In this study, the alloy $S_{70}Se_{30-X}Pb_X$ will be prepared with the ratios x = (0, 5, 10, 15) using the melting point method and studying the effect of partial replacement of selenium with lead on the electrical properties and density of states within the energy gap and in the conduction and valence bands.

MATERIALS AND METHODS

Five samples of the alloy $S_{70}Se_{30-x}Pb_x$ were prepared with the ratios x = (0, 5, 10, 15) and partial replacement of selenium with lead using the melting point method according to the following procedures:

$$70\ S + (30-x)\ Se + x\ Pb = Se_{70}Se_{30-x}\text{-}Pb_x \quad (1)$$

The alloys were prepared from their constituent elements (sulfur (S), selenium (Se) and lead (Pb)) with high purity (99.999%). The elements that make up the alloy were weighed according to the specified weight ratio. The alloys were prepared by partial replacement of selenium with lead in specific proportions, namely X (0, 5, 10, 15). The components of the above-mentioned chemical compounds were mixed and crushed, and each compound was placed in a plastic container. To avoid any reactions between the alloy elements and oxygen at high temperatures, each sample was placed in quartz tubes and closed after being evacuated using a vacuum to remove the air from inside them until the pressure reached 10^{-3} Pa. After that, the vacuum capsules were placed in the electric oven at 350 degrees Celsius, and the oven temperature was gradually increased by 10 degrees Celsius every minute, and the samples were kept for 3 hours. After that, the electric oven was turned off and the capsules were left inside the oven to cool slowly and gradually for 24 hours. After that, the capsules were extracted from the electric oven and the glass tubes were broken on waxed paper to extract the molten material very carefully and extract the material from each capsule individually. After that, the components of each sample were crushed until the samples were ready for pressing using a hydraulic press. They were formed into small discs under an approximate force of 7 tons/cm², which led to the production of discs with dimensions of 1.5 cm in diameter and 0.4 cm in thickness according to their concentration. Each disc was connected in an electrical circuit with two poles attached to a device (digital ohmmeter) that applies a certain voltage difference between the two ends of the sample and automatically measures the amount of current passing through the sample, and via an electronic screen in the digital ohmmeter, the amount of resistance appears. The samples were placed separately in the oven. The effect of electrical resistance was studied with a change in temperature from 24 to 200 degrees Celsius.

RESULTS AND DISCUSSION

The current-voltage (I-V) characteristics of the $S_{70}Se_{30-x}Pb_x$ glass alloy were examined within a temperature range of 297-473 Kelvin to study changes in the electrical conductivity of direct current. Through these measurements, the electrical resistivity and then the conductivity were calculated for all studied samples. The dependence of electrical conductivity on temperature was analyzed by comparing the results obtained according to the replacement ratio of the samples. The logarithmic relationship between electrical conductivity and temperature is shown in Figure 1, which shows how the electrical conductivity Ln (σ) and 1000/T change. The data show that all samples follow semiconductor behavior, where the conductivity increases exponentially with increasing temperature [18, 19].

At low temperatures (297-353 K), charge carriers gain enough energy to transition between localized states near the Fermi level. This process takes place at a relatively low activation energy, gradually increasing conductivity [14, 20]. However, above 353 K, charge carriers become more mobile, allowing conduction to occur via band-tail hopping. In the range of 353 K to 423 K, conduction is mainly driven by the variable-range-hopping (VRH) mechanism. At high temperatures, between 423 K and 473 K, conduction is dominated by a thermally assisted process. This process involves the transition of electrons between extended states in the conduction and valence bands. The observed behavior is consistent with the theoretical predictions shown in Eq. 2 [4, 14, 15].

$$\sigma = \sigma_{01} e^{\left(-\frac{E_1}{KT}\right)} + \sigma_{02} e^{\left(-\frac{E_2}{KT}\right)} + \sigma_{03} e^{\left(-\frac{E_3}{KT}\right)} \quad (2)$$

The slopes of the curves were analyzed in three thermal regions, namely low (297–353) K, medium (353–423) K, and high (423–473) K, to determine the activation energies (E1, E2, E3) and the pre-exponential factor (σ_{01}, σ_{02}, σ_{03}) of the $S_{70}Se_{30-x}Pb_x$ glass alloy. Table 1 shows the calculated values of the pre-exponential factor (σ_o), which reveal important insights into the conduction mechanisms in chalcogen glasses. The curves indicate the existence of five separate paths, each characterized by a different slope associated with a specific activation energy. According to Equation (1), the slope of the graph of ln σ versus 1000/T can be used to determine the activation energies (E1, E2, E3). According to the substitution ratio [21, 22], the equation also allows the calculation of the pre-exponential factors

(σ_{01}, σ_{02}, σ_{03}) within the three temperature ranges. These factors can be determined from the length of the curves and their points of intersection with the axis [23, 24]. The calculated values of these factors are shown in Table 1.

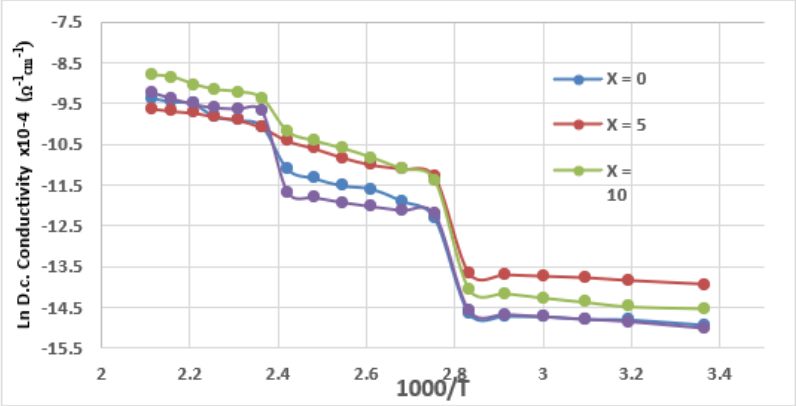

Figure 1, The relationship between Ln (σ) and 1000/T for $S_{70}Se_{30-x}Pb_x$ alloy with x = 0, 5, 10, and 15

Table 1 shows the σ as a function of Lead concentration alloy with x = 0, 5, 10, and 15

x	σ_o ext	$\sigma_{o\ loc}$	$\sigma_{o\ fermi}$
0	8.53048E-05	4.26524E-05	4.32706E-07
5	6.63482E-05	4.14676E-05	1.14833E-06
10	0.000149283	8.41033E-05	7.85702E-07
15	9.95223E-05	6.22014E-05	4.59334E-07

The data also indicates a nonlinear relationship between σ and 1000/T, which arises from multiple defects at grain boundaries due to imperfect atomic bonding. These defects lead to the trapping of charge carriers at low temperatures. At the same time, the density of states near the Fermi level improves the mobility of carriers at high temperatures by reducing the trapping states and potential barriers [24, 25]. Figure (2) shows the relationship between the energy tail width values (ΔE = E1- E2) and the partial substitution ratio and according to the Pb substitution [26-28],

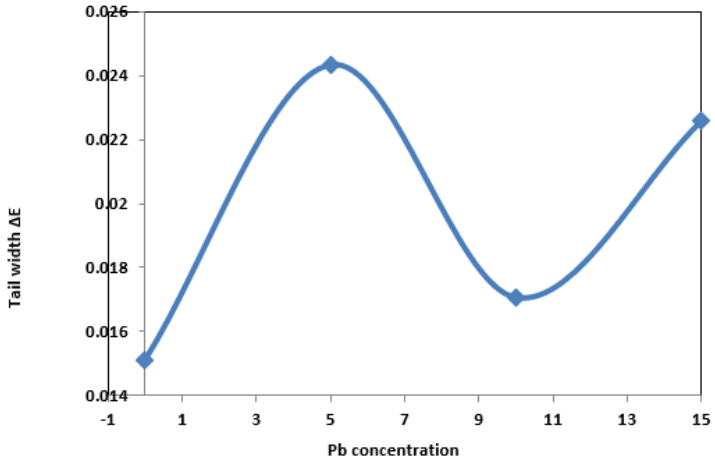

Figure 2 shows the relationship between the energy tail width values (ΔE = E1- E2) vs Pb concentration

It was noted from Figure 2 that, width of the energy tail (ΔE) changes with the change in the lead concentration. At first, when x = 0, the width of the energy tail ΔE is low, then it starts to rise with the increase in the value of x to its highest value at x = 5. Then it starts to decrease after that to lower values at 0 x = 1, after that it starts to increase. This indicates that the decrease in the width of the tail means a decrease in randomness, i.e., an increase in the crystallization state, as this value is considered the ideal state [29]. To calculate the energy state densities in three different regions:

localized N (E_{loc}), extended N (E_{ext}), and Fermi level N (E_F). According to the ratio of substitution of the values of the constants (electron charge e, electron mass and values σ_{01}, σ_{02}, σ_{03}) in the equations in references [13, 14] mentioned below, the energy state densities in three different regions - local, extended, and Fermi level - were calculated. According to the following equations:

$$N(E_{ext}) = \left[\frac{6m}{e^2\hbar}\right] \sigma_{oext.} \quad (3)$$

$$N(E_{loc}) = \left[\frac{6}{e^2 . f_{phonon} . R^2}\right] \sigma_{0\,loc} \quad (4)$$

$$N(E_F) = \left[\frac{6}{e^2 f phonon\, R^2}\right] \sigma_{o3} \quad (5)$$

Where $\hbar = 1.0545 \times 10^{-34}$ J.s f_{ph} is the phonon frequency, which is of order 10^{13} $s^{-1}$and R is the hopping distance and is , given by $R = 0.7736\left[\frac{\Delta E a^{-1}}{N(E_C)(KT)^2}\right]^{0.25}$ and $a^{-1} = 10$ A.

The three equations 3, 4, 5 were applied to calculate both the extended and localized state densities and at the Fermi level after substituting the constants in the equations. The values calculated from these equations were recorded in Table 2.

Table 2 shows the relationship between the density of extended states N(E_{ext}), N(E_{loc}), N(E_{fermi}) and upon partial substitution of selenium by lead

x	Tail Width ΔE (ev)	R (A^0)	a (A^0)	N(E_{ext}) ($ev^{-1}cm^{-3}$)	N(E_{loc}) ($ev^{-1}cm^{-3}$)	N(E_F) ($ev^{-1}cm^{-3}$)
0	0.015123519	0.893410845	1.18542	4.40381E+21	1.25243E+21	11182152
5	0.024352764	1.07167029	1.52412	3.42518E+21	8.46249E+20	225435.559
10	0.017065306	0.800584198	6.77386	7.70666E+21	3.07546E+21	1028640.016
15	0.022603374	1.07167029	1.52412	5.13777E+21	1.6137E+21	8806076.525

Figure 3 and Table 2 show that the density of extended states changes as the lead concentration increases from 0, 5, 10, and 15, and reaches its highest value at concentration 10, at which it equals 7.70666E+21(ev-1cm-3), and then decreases at 15. This is attributed to several factors, such as the change in the mobility gap, the width of the energy tails, the concentration of the conductive materials, or a change in the conductive properties [12, 18, 19].

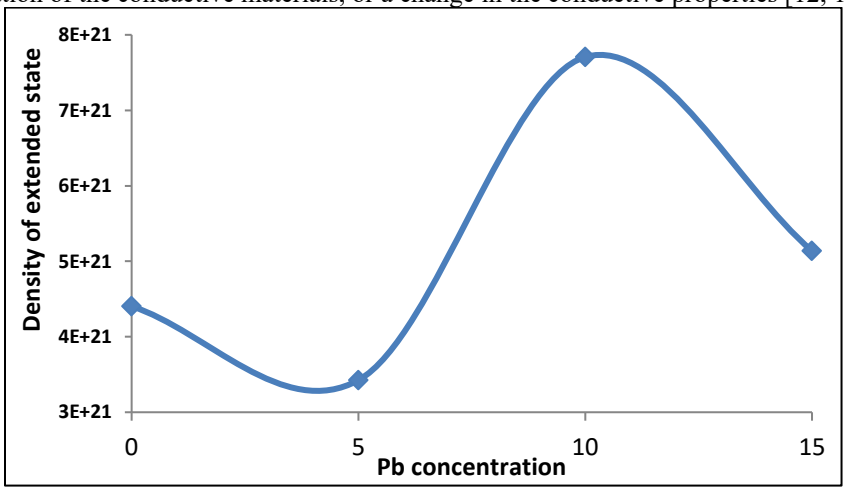

Figure 3 shows the Density of extended states N($E_{ext.}$) as a function of Pb concentration

Figure 4 shows the relationship between the density of local states and the concentration of lead. It is noted from this figure that the density of local states changes with increasing concentration of lead, as it decreases to its lowest value at concentration 5, then reaches its highest value at concentration 10 where it equals 3.07546×10^{21} ($ev^{-1}cm^{-3}$), and after

that the density of local states decreases with increasing concentration of lead. This is attributed to several factors, such as changing the conduction gap, the width of the energy tails, the concentration of the conductive material, or a change in the properties of the conductor [30].

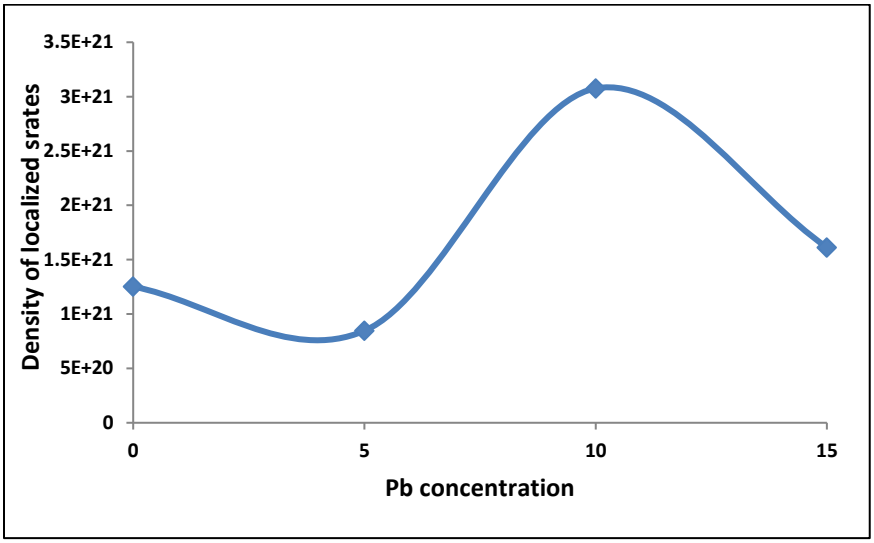

Figure (4) shows the Density of extended states $N(E_{loc.})$ as a function of Pb concentration

Figure 5 represents the relationship between the density of states at the Fermi level and the lead concentration. At first, it is noted that there is a decrease in the density of states at the Fermi level when the lead concentration value increases from 0 to 5 to reach its lowest value of 225435.559 ($eV^{-1}cm^{-3}$) and then these values increase when the concentration rises at x=15.

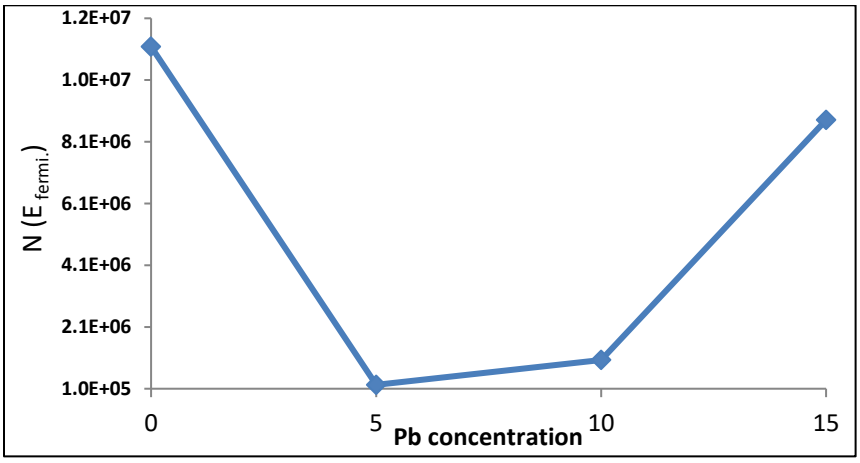

Figure 5 shows the Density of localized states at firmi level N (E_{Fermi}) as a function of Pb concentration

It was found from these results that the best density of states is when the concentration of lead is (Pb = 10) because the energy gap is small at the extended levels at this concentration, to take the preferred value. Also note that the energy levels of all extended and localized states and at the Fermi level change with the change in concentration, as these levels depend on the strength of the bond between the atoms [25]. The more the bonds are equivalent and interconnected with each other, the less randomness in the crystal structure and the higher the percentage of crystallization in the alloys. When the percentage of lead changes, it leads to a change in the width of the tails of the bundles, and this change in the width of the tails of the bundles leads to pulling it outside the energy gap, it becomes one of the extended states. As for increasing the tails of the bundles, this leads to the extension of these tails within the energy gap [26], as indicated by the researchers [4, 5]. From this, we conclude that the process of partial replacement of selenium with the element lead led to the ability to control the reduction or increase in randomness

depending on the ability of the bonds with which the lead bonds[27]. If the bonding process is high, the randomness decreases and the crystallinity increases. Conversely, if the dangling bonds in the alloy increase, the randomness will increase, which leads to an increase in irregularity and thus an increase in the density of local states at the Fermi level. This is because the valence bands in chalcogenide glasses have a high percentage of electronic states (unshared) which are called lone pairs and the process of substitution or introduction of other elements in chalcogenide alloys where the valence electrons close to the more electronegative atoms have higher energies than those located near the atoms with a high electrical charge, it has been observed that partial substitution affects the width or narrowing of the tail of the bands and the width may be similar to the valence bands and the tail of the bands changes as a result of the increasing or decreasing types of bonds in the alloys and this may lead to an increase or decrease in the edge of the conduction or valence band, which affects the densities of local and extended state.

CONCLUSION

This study deals with the effect of partial substitution on the density of local, extended and Fermi level states in $S_{70}Se_{30-x}Pb_x$ alloy by the melting point method and at x ratios (0, 5, 10, 15). By analyzing the electrical conductivity across different temperature ranges, three distinct conduction mechanisms were identified, related to the extended states $N(E_{ext})$, local $N(E_{loc})$ and Fermi level ($N(E_F)$ at high temperatures between (423 K and 473 K), medium temperatures between (353 K and 423 K) and low temperatures between (297-353 K) respectively. The results showed that all the densities of these states are significantly affected by the substitution ratio. This is due to the movement of carriers between the extended states in the conduction and valence bands as well as due to the change in the width of the energy tails, the hopping distance of the electrons, as well as the activation energy. The density of the three states. The electrical conductivity constants, the energy band gap, the tail width ΔE, the hopping distance between two local states R, and the distance between atoms a were calculated. It was found that all of them change with the change in the concentration of the lead element.

REFERENCES

1. Tohge, N., Matsuo, H., & Minami, T. (1987). Electrical properties of N-type semiconducting chalcogenide glasses in the system Pb-GE-Se. Journal of Non-Crystalline Solids, 95-96, 809-816. https://doi.org/10.1016/s0022-3093(87)80685-3
2. .Tohge, N., Kanda, K., & Minami, T. (1986). Formation of chalcogenide glass p-n junctions. Applied Physics Letters, 48(25), 1739-1741. https://doi.org/10.1063/1.96820
3. Street, R. A., & Mott, N. F. (1975). States in the gap in glassy semiconductors. Physical Review Letters, 35(19), 1293-1296. https://doi.org/10.1103/physrevlett.35.1293.
4. Shore, K. A. (2014). Electronic processes in non-crystalline materials (Second edition), by N.F. Mott and E.A. Davis. Contemporary Physics, 55(4), 337-337. https://doi.org/10.1080/00107514.2014.933254.
5. Mott, N. (1972). Introductory talk; Conduction in non-crystalline materials. Journal of Non-Crystalline Solids, 8-10, 1-18. https://doi.org/10.1016/0022-3093(72)90112-3Vikhrov.
6. S., Nagels, P., & Bhat, P. K. (1981). N-type conduction in Chalcogenide glasses of the GE-se-Bi system. Recent Developments in Condensed Matter Physics, 333-340. https://doi.org/10.1007/978-1-4684-3899-4_42.
7. Tohge, N., Minami, T., & Tanaka, M. (1983). Photoconductivity of vitreous chalcogenides chemically modified by bismuth. Journal of Non-Crystalline Solids, 59-60, 999-1002. https://doi.org/10.1016/0022-3093(83)90335-6.
8. Mohammed, J. S., Nsaif, F. K., Jawad, Y. M., Jasim, K. A., & Al Dulaimi, A. H. (2023). Investigating the optical and electrical characteristics of as60cu40-xsex thin films. Chalcogenide Letters, 20(7), 449-458. https://doi.org/10.15251/cl.2023.207.449.
9. Jasim, K. A., Makki, S. A., & Almohsin, A. A. (2014). Comparison study of transition temperature between the superconducting compounds Tl0.9 Pb0.1 ba2ca2cu3o9-δ, tl0.9sb0.1ba2ca2cu3o9-δ and tl0.9cr0.1ba2ca2cu3o9-δ. Physics Procedia, 55, 336-341. https://doi.org/10.1016/j.phpro.2014.07.049.
10. Ahmed, B. A., Mohammed, J. S., Fadhil, R. N., Jasim, K. A., Shaban, A. H., & Al Dulaimi, A. H. (2022). The dependence of the energy density states on the substitution of chemical elements in the se6te4-xsbx thin film. Chalcogenide Letters, 19(4), 301-308. https://doi.org/10.15251/cl.2022.194.301.
11. Khudhair, N. H., & Jasim, K. A. (2023). Study the effect of tin on the energy density of states of Se60Te40-xSnx chalcogenide glass. AIP Conference Proceedings, 2769, 020062. https://doi.org/10.1063/5.0129373.
12. Khudhair, N. H., & Jasim, K. A. (2023). Preparation and study the effective of Sb on the energy density of states of Se60 Te40. AIP Conference Proceedings, 2769, 020056. https://doi.org/10.1063/5.0129550.

13. Khudhair, N. H., & Jasim, K. A. (2023). A study of the effectiveness of tin on the thermal conductivity coefficient and electrical resistance of Se60Te40-xSnx Chalcogenide glass. Ibn AL-Haitham Journal For Pure and Applied Sciences, 36(1), 149-157. https://doi.org/10.30526/36.1.2892.
14. Abdulateef, A. N., Alsudani, A., Chillab, R. K., Jasim, K. A., & Shaban, A. H., "Calculating the Mechanisms of Electrical Conductivity and Energy Density of States for $Se_{85}Te_{10}Sn_{5-x}In_x$ Glasses Materials", Journal of Green Engineering 10 (2020) 5487-5503.
15. Chillab, R. K., Jahil, S. S., Wadi, K. M., Jasim, K. A., & Shaban, A. H. (2021). Fabrication of Ge30Te <sub>70-xSbx Glasses alloys and studying the effect of partial substitution on D.C electrical energy parameters. Key Engineering Materials, 900, 163-171. https://doi.org/10.4028/www.scientific.net/kem.900.163
16. Jasim, K. A., & Alwan, T. J. (2017). Effect of oxygen treatment on the structural and electrical properties of Tl0.85Cd0.15Sr2CuO5−δ, Tl0.85Cd0.15Sr2Ca2Cu2 O 7−δ and Tl0.85Cd0.15Sr3Ca2Cu3 O 9−δ superconductors. Journal of Superconductivity and Novel Magnetism, 30(12), 3451-3457. https://doi.org/10.1007/s10948-017-4147-9.
17. Neamah, Z. J., Ahmed, B. A., Thejeel, M. A., Jasim, K. A., & Shaban, A. H. (2022). The effect of gamma radiation on the manufactured $HgBa_2Ca_2Cu_{2.4}Ag_{0.6}O_{8+\delta}$ Compound. Materials Science Forum, 1050, 41-47. https://doi.org/10.4028/www.scientific.net/msf.1050.41
18. Adler, D. (1975). Disordered materials: Amorphous and liquid Semiconductors. J. Tauc, ed. Plenum, New York, 1974. X, 442 pp., illus. $28. Science, 188(4184), 141-142. https://doi.org/10.1126/science.188.4184.141.b.
19. Jasim, K. A. (2012). The effect of cadmium substitution on the superconducting properties of $Tl_{1-x}Cd_x$ $Ba_2Ca_2Cu_3O_{9-\delta}$ compound. Journal of Superconductivity and Novel Magnetism, 26(3), 549-552. https://doi.org/10.1007/s10948-012-1787-7
20. Lee, J., Park, S. D., Kim, B. S., Oh, M. W., Cho, S. H., Min, B. K., Lee, H. W., & Kim, M. H. (2010). Control of thermoelectric properties through the addition of Ag in the Bi0.5Sb1.5Te3 alloy. Electronic Materials Letters, 6(4), 201-207. https://doi.org/10.3365/eml.2010.12.201.
21. Mobarak, M., Shaban, H., & Elhady, A. (2008). Electrical and thermoelectric properties of CuInS2 single crystals. Materials Chemistry and Physics, 109(2-3), 287-290. https://doi.org/10.1016/j.matchemphys.2007.11.025.
22. Aleabi, S. H., Watan, A. W., Salman, E. M., Jasim, K. A., Shaban, A. H., & AlSaadi, T. M. (2018). The study effect of weight fraction on thermal and electrical conductivity for unsaturated polyester composite alone and hybrid. AIP Conference Proceedings, 1968, 020019. https://doi.org/10.1063/1.5039178.
23. Al-Khafaji, R. S., & Jasim, K. A. (2021), AIMS Materials Science, 8(4), 550-559. https://doi.org/10.3934/matersci.2021034.
24. Paul, D. K., & Mitra, S. S. (1973). Evaluation of Mott's parameters for hopping conduction in amorphous GE, SI, and Se-SI. Physical Review Letters, 31(16), 1000-1003. https://doi.org/10.1103/physrevlett.31.1000.
25. M. Julian and C. Salame, “Energy management, critical analysis and recommendations: Case study Lebanon,” Energy Rep. 8, Suppl. 9, 1063–1075 (2022).
26. M. Palivos, G. A. Vokas, A. Anastasiadis, P. Papageorgas, and C. Salame, “Comparison study of the technical characteristics and financial analysis of electric battery storage systems for residential grid,” AIP Conf. Proc. 1968, 030076 (2018).
27. K. Agavanakis, P. G. Papageorgas, G. A. Vokas, D. Ampatis, and C. Salame, “Energy trading market evolution to the energy internet: a feasibility review on the enabling Internet of Things (IoT) cloud technologies,” AIP Conf. Proc. 1968, 030077 (2018).
28. Wadi, K.M., Jasim, K.A., Shaban, A.H., Kamil, M.K., Nsaif, F.K., The effects of sustainable manufacturing pressure on the structural properties of the pb2ba2ca2cu3o9+σ compound, Journal of Green Engineering, 2020, 10(9), pp. 6052–6062.
29. Omar, B. A., Fathi, S. J., & Jassim, K. A. (2018), Effect of Zn on the structural and electrical properties of high temperature HgBa2Ca2Cu3O8+δ superconductor. AIP Conference Proceedings, 1968, 030047. https://doi.org/10.1063/1.5039234.
30. Thouless, D. J. (1980). Disordered materials: Electronic processes in non-crystalline Materials. N. F. Mott and E. A. Davis. Second edition. Clarendon (Oxford University Press), New York, 1979. xiv, 590 pp., illus. $65. The international series of monographs on physics. Science, 207(4436), 1196-1197. https://doi.org/10.1126/science.207.4436.1196-b.